Ultrasonics 94 (2019) 401–410

Contents lists available at ScienceDirect

Ultrasonics

journal homepage: www.elsevier.com/locate/ultras

Self-sensing cavitation detection in ultrasound-induced acoustic cavitation

Kai-Alexander Saalbach*, Jens Twiefel, Jörg Wallaschek

Institute of Dynamics and Vibration Research, Leibniz Universität Hannover, Appelstraße 11, 30167 Hannover, Germany

ARTICLE INFO

Keywords:
Ultrasound
Cavitation detection
Acoustic cavitation
Self-sensing

ABSTRACT

The generation of cavitation by ultrasound is used in a large number of processes in different scientific and industrial applications. Chemical reactions are made possible or accelerated by locally occurring high temperatures and pressures generated by the collapse of cavitation bubbles. Mixing or separating substances, emulsification, ultrasonic cleaning, degassing, and microbiological treatment of fluids are some more applications for ultrasonic generated cavitation. In most of these applications, an optical examination of the events within the cavitating medium is not possible. Non-transparent media or closed containers prevent an optical process monitoring. In addition, the use of sensors is often impossible for cost reasons, limited construction space or disturbance of the process. In order to still enable process monitoring, the authors follow a novel approach: the analysis of the electrical signals of the ultrasound transducer used for cavitation generation. The current signal of the ultrasound transducer is inspected for frequency components, known as acoustic cavitation indicators. For this, the time signal is recorded and transferred to the frequency domain for further processing and evaluation. In previous studies, acoustical sensors like hydrophones or microphones were used as reference for the self-sensing technique.

In order to link cavitation events inside the fluid container to cavitation indicators in the current signal, a photo study of the cavitation events inside a transparent water container is conducted. In contrast to previous self-sensing attempts, the ultrasound transducer's transfer characteristic is also considered. The evaluation of the acquired data shows that a frequency component which is 3/2 times the driving frequency (~30 kHz) can be used to determine the onset of transient cavitation. Once the transient cavitation threshold has been exceeded, broad band noise levels show a good correlation with cavitation intensity.

1. Introduction

The generation of cavitation can be beneficial to many processes. The motivation for the application of the presented self-sensing approach is an industrial application: the manufacturing of heat sinks during casting. The aim of this process is to generate a cohesive connection between aluminum and copper, both of which have good thermal conductivity and are commonly used in the production of heatsinks. The authors' approach to enable the connection between aluminum and copper is to apply ultrasound to the melt in order to generate cavitation [1]. The cavitation bubbles then clean the surface of the solid copper part and destroy oxide layers, which prevent a connection. The described ultrasonically assisted casting process leads to a cohesive bond [2], ensuring high thermal conductivity.

In order to control this manufacturing process, a method for monitoring cavitation is needed. The casting mould and aluminum melt provide an opaque environment, thus making optical process monitoring impossible. In addition, the use of measurement equipment, like hydrophones, is impossible due to the high temperature of the liquid. Yet, in order to provide process monitoring, the electrical signals of the ultrasound transducer, used to create cavitation, can be analyzed for indicators in the frequency domain. The working principle of this self-sensing technique has already been successfully tested [3–6]. The principle is based on the fact that different frequency portions, known as acoustic indicators for cavitation [7,8], can also be found in the electrical signals of the transducer. These indicators can be the noise level or frequencies related to the ultrasonic driving frequency f_0. The driving frequency related indicators can be divided into harmonics ($n*f_0$), subharmonics (f_0/n) and ultraharmonics ($n*f_0/m$, $m = 2, 3, 4, \ldots$) with n being the harmonic index ($n = 2, 3, 4, \ldots$). Broadband noise is known as an indicator for transient cavitation. Commonly used devices for cavitation monitoring are additional transducers [9], passive piezoelectric receivers [10], microphones [11,12] or hydrophones [13,15]. The investigations, applying the self-sensing concept, link different indicators to cavitation events. In [3] the frequency portions $3/2f_0$, $5/2f_0$ and $7/2f_0$ are associated to the onset of transient

* Corresponding author.
E-mail addresses: saalbach@ids.uni-hannover.de (K.-A. Saalbach), twiefel@ids.uni-hannover.de (J. Twiefel), wallaschek@ids.uni-hannover.de (J. Wallaschek).

https://doi.org/10.1016/j.ultras.2018.06.016
Received 14 July 2017; Received in revised form 4 June 2018; Accepted 26 June 2018
Available online 28 June 2018
0041-624X/

cavitation. By comparison with the signals from a special cavitation sensor, in [4,5] different subharmonic and ultraharmonic frequency components in the current signal are investigated for their suitability for cavitation detection. The components $3/2f_0$, $7/3f_0$, $3.9f_0$ and $4.2f_0$ are presented as possible indicators for the onset of stable and transient cavitation. A sudden change in resonance frequency is also found to agree with the occurrence of transient cavitation. Although the thresholds for the onset of transient cavitation could not be detected with the frequency components $5/2f_0$ and $7/2f_0$, these two portions are suspected to be related to the strength of cavitation. Furthermore, the effect of changes of the experimental setup is investigated. The exchange of the ultrasonic transducer or the driving electronics changes the self-sensing results. For one type of setup the intensity of ultraharmonics is linked to the strength of cavitation.

Instead of monitoring indicators in the frequency domain, another approach is to evaluate changes in the transducers impedance. In this way the volume fraction of gas in the vicinity of the transducer can be related to the transducer's impedance [14,16].

In this contribution, a laboratory setup is used to investigate the dependence of cavitation indicators on ultrasound intensity and the corresponding cavitation events within the medium.

First the principle of self-sensing cavitation detection is explained. Then the experimental setup is presented and experimental results are shown. Before the results are discussed, the measurement results are evaluated, to find a correlation between cavitation intensity and frequency based indicators.

2. Principle of cavitation detection

Before the experimental setup and the results are described, the principle of cavitation detection, applied here, will first be explained. The ultrasound transducer is actually a piezoelectric converter that converts electrical alternating signals into mechanical vibrations, which in turn excite the surrounding fluid and generate a sound field. In order to create a high mechanical amplitude, that generates high pressure in liquids, to thus generate cavitation, the transducer is driven at resonance in its third longitudinal eigenmode. The cavitation bubbles in the fluid produce mechanical deformation on the transducer's horn, which leads to a deformation of the piezo elements of the converter, which in turn generate electrical signals. These signals are small compared to the driving signal and are superimposed on it. The superimposed signals can be recognized by measuring the transducer's current signal and transferring it to the frequency domain. The principle described is shown graphically in Fig. 1(a). The sound wave generated by the converter and amplified by the transducer's geometry is depicted in black. The vibrations resulting from the deformation, caused by the bubbles, are shown in gray. The challenge of self-sensing cavitation detection can be made clear by Fig. 1(b), in which an electrical equivalent circuit of a piezoelectric transducer, driven near a resonance frequency, coupling the electric, mechanical and acoustic domain, is shown. This simplified model is based on the equivalent circuit model by Van Dyke [15]. In the electrical domain, the voltage U and current i are the electrical signals driving the converter and C_P is the transducer's piezoelectric parallel capacitance. The term $1{:}\alpha$ represents the mechanical transmission factor, coupling the electrical and mechanical domain, in which C_m, L_m and R_m correspond to the transducer's stiffness, mass and attenuation respectively.

Z_L is the changing load impedance, representing the process. It is part of the acoustic domain, which is coupled to the mechanical domain by the transmission factor $1{:}\beta$. For the presented self-sensing approach, voltage U and current i are measured at the converter's terminals.

For a steady state system, like the one depicted, and a constant load the determination of the system behavior and the systems' parameters is straightforward.

The system behavior of a power ultrasound transducer and its application in cavitation generation is more complex. Since for amplitude increase, the length of the ultrasound system is tuned to the wavelength of the operating frequency, further multiples of this frequency are excited in addition to the operating frequency. This generates additional content in the frequency domain, which makes the identification of cavitation induced frequency portions more difficult. Furthermore, a cavitating liquid is a complex transient load, varying temporally and locally. Therefore, a model based approach for cavitation detection is difficult and experimental investigation has to be conducted.

3. Experimental setup

For studies on the cavitation events inside the fluid container, a transparent laboratory setup was used at room temperature. Water was selected as a transparent liquid. A transparent cylindrical water container (inner diameter 110 mm) made of polymethyl methacrylate (PMMA) was used for the experiments. A cover with a hole in its center was put on the container, to position the transducer at the center of the container. With this setup, a camera was used to take pictures of the cavitation events. The amount of water in the container was held constant throughout the experiments.

An ultrasound transducer (tip diameter 30 mm), driven at its third longitudinal natural frequency (approximately 20.64 kHz), was used to generate the sound field within the fluid and thereby create cavitation. A power amplifier (QSC RMX 4050), as well as frequency and amplitude control hardware, (DPC 500/100 k) [16] were used to drive the transducer. With a digital oscilloscope (Picoscope5203) connected to a PC, the voltage and current signals at the transducer's terminals were recorded, using a voltage-probe (Testec TT-HV 15) and a current-probe (Tektronix P6021). The camera (Nikon D3100 + Sigma DC 18–250 mm lense) was also connected to the PC for triggering. With a measurement routine, datasets were recorded over a time span defined by the number of samples and the samplingrate. Each dataset consists of 20 kSample blocks with 1 MSample sampling rate of the electrical signals, and a photo taken with an exposure time of 1/1000 s.

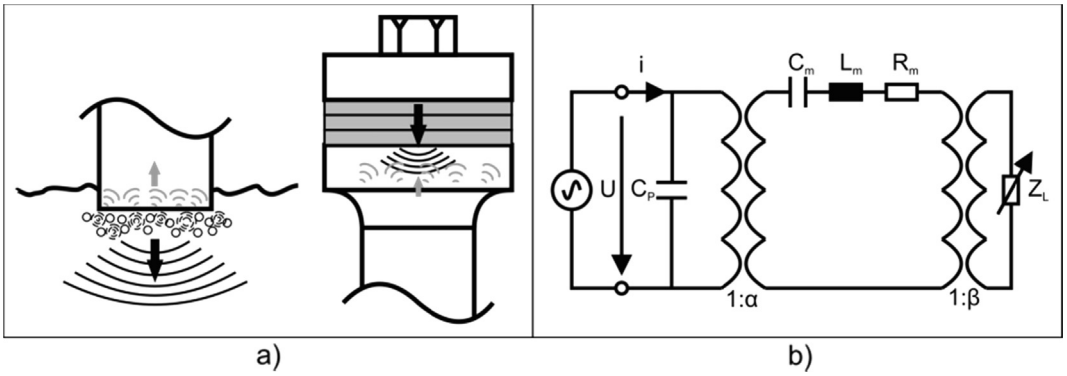

Fig. 1. Principle of self-sensing: (a) Reaction of the cavitation bubbles on the transducer; (b) Equivalent circuit of Transducer with changing load.

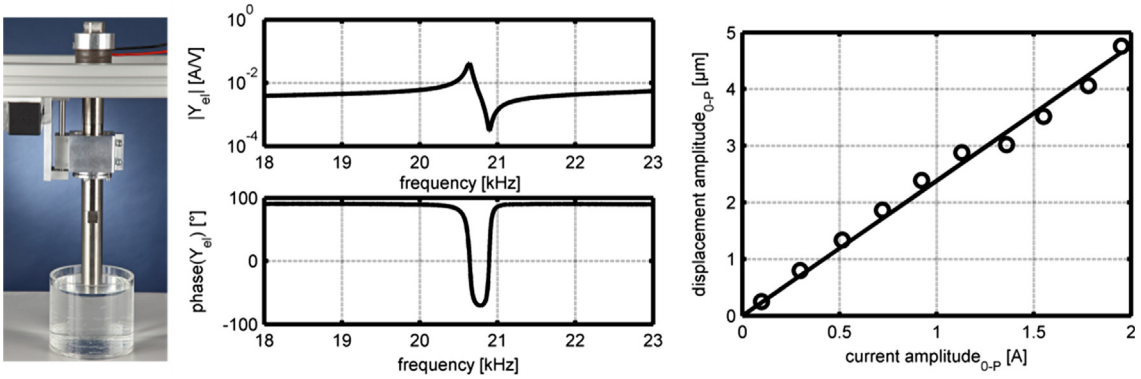

Fig. 2. Photo of the mounted transducer, transducers's frequency response ($|Y_{el}|$ and phase (Y_{el})) and current amplitude - displacement amplitude characteristic.

The mounted transducer, used in the experiments, its measured frequency response (admittance $|Y_{el}|$ and phase (Y_{el})), and its current-displacement characteristic are shown in Fig. 2. Using the frequency response measurement, the resonance frequency, used for driving the transducer, can be determined to be approximately 20.64 kHz. This measurement was conducted in air without a load. By compensating the transducer's parallel capacitance C_P [17,18], and computing the mechanical phase value phase (Y_{mech}), the control hardware drives the transducer at the displayed frequency characteristic independent of the load.

For an ultrasound transducer driven at a resonance frequency the displacement amplitude is proportional to the amplitude of the driving current. The mechanical transmission factor α was measured with a fiber-optic laser vibrometer (Polytec OFV-552 and vibrometer controller OFV-5000) at the tip end of the transducer's horn. Because the excitation frequency was measured as well, the displacement amplitude is calculated based on the velocity measurement.

4. Results

The experimental setup was used to generate cavitation in water, in order to investigate the dependence of frequency portions in the transducer's current signal on the excitation displacement amplitude and the cavitation events inside the liquid. For this purpose, the immersion depth (distance between the horn's tip and the bottom of the water container) and the vibration amplitude were varied. Measurements were made for four different distances (65 mm, 70 mm, 75 mm, 80 mm) with current amplitudes increasing from 100 mA to 2000 mA in 100 mA intervals. Spectrograms of the current signal were computed from the recorded electrical data, showing the frequency content over time. The photos taken during the measurements were processed for determination of the bubble content.

4.1. Spectrograms

Different frequency components in the current signal of the transducer are used for the indication of cavitation events. The signals resulting from the reaction of the cavitation bubbles on the horn are small compared to the driving signal. In order to be able to recognize the cavitation related signal components, amplitudes of up to 5 mA are displayed in the spectrograms. By limiting the amplitude range and adjusting the displayed color spectrum to the interval 0–5 mA, higher values are truncated. The investigation of the frequency spectrum showed that the major changes, which are considered cavitation related, occur in the range up to 100 kHz, therefore the spectrograms are limited to this range. In order to obtain an impression of which frequency components are generated at different excitation amplitudes, Fig. 3 shows spectrograms for five current values for a distance of 80 mm between the bottom of the container and the horn's tip. For 100 mA, 500 mA and 1000 mA only the driving frequency f_0 and its harmonics show elevated amplitude values with rising intensity. In the spectrograms for 1500 mA and 2000 mA further frequency components can be found. The most pronounced frequency components are the $3/2f_0$ (~30 kHz) and the $5/2f_0$ (~50 kHz) portion. In addition to the numerous frequency portions, the global noise level is also higher in comparison to the lower current intensities. This is indicated by the brighter blue[1] tone between the single pronounced frequencies. Additionally, a low frequency component of approximately 50–100 Hz becomes visible from the 1000 mA spectrogram.

The measurements presented in Fig. 3 show the cavitation generated frequency components superimposed on the frequency content generated by the transducer itself. In order to be able to distinguish between these two sources, it is necessary to investigate the frequency components which are generated by the transducer without a load. For this investigation the experimental setup was used without submerging the horn's tip in water. For different excitation amplitudes the electrical signals were recorded and spectrograms were computed from the measured data. Results of these measurements are shown in Fig. 4. For good comparability spectrograms for the same excitation amplitude as in Fig. 3 are shown. While the 100 mA spectrogram mainly shows pronounced values for the driving frequency (~20.6 kHz), the spectrograms for higher amplitudes also show elevated values for the harmonics of the driving frequency. The low frequency component, already found in the spectrograms measured under load conditions, is also present. In the 2000 mA spectrogram even the global noise level rises. The results of the measurements with the unloaded transducer show that the transducer itself generates frequency portions that are similar to known cavitation indicators: the harmonics of the driving frequency and a low frequency component. In addition, an elevated noise level is generated by the transducer itself. Therefore, these components cannot be used as indicators for cavitation activity for the presented setup. Since the frequency components that arise during cavitation generation and the characteristic frequency components of the transducer are known, the next step is to find out what occurs in the liquid. This is done be evaluating the photos taken during the measurements.

4.2. Photo study

Photos were taken to monitor the events inside the fluid during each measurement, and one photo for each dataset of the electrical signals was taken. This results in one photo for every time-step of the spectrograms. To ensure the best quality photos, the lighting was aligned so that the light fell through the contents of the vessel towards the camera. This enabled cavitation bubbles to be detected due to a change in the

[1] For interpretation of color in Fig. 3, the reader is referred to the web version of this article.

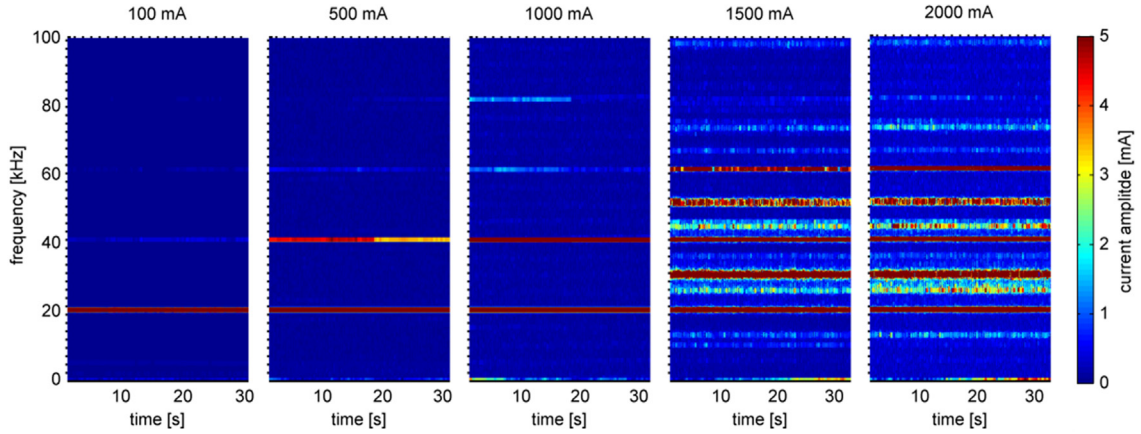

Fig. 3. Spectrograms of transducer's current signal for different current amplitudes at 80 mm distance.

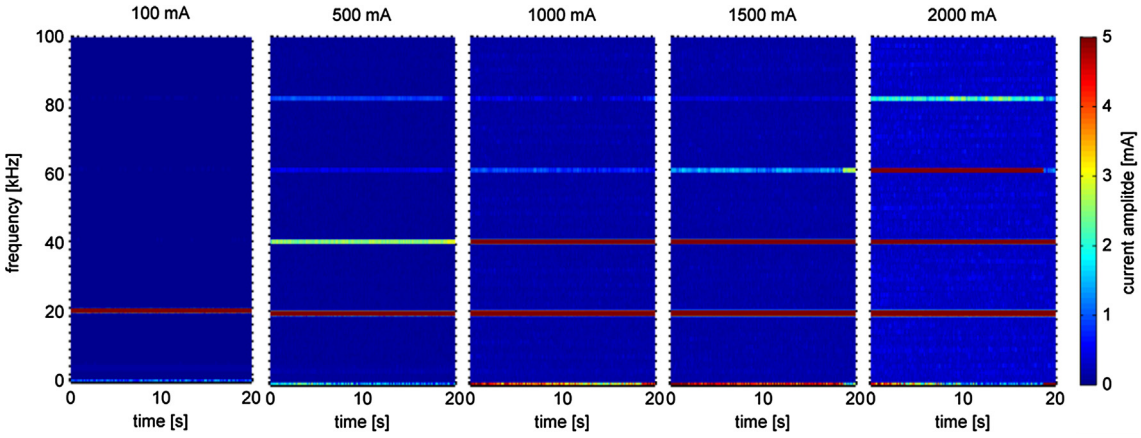

Fig. 4. Spectrograms of transducer's current signal for different current amplitudes without load in air.

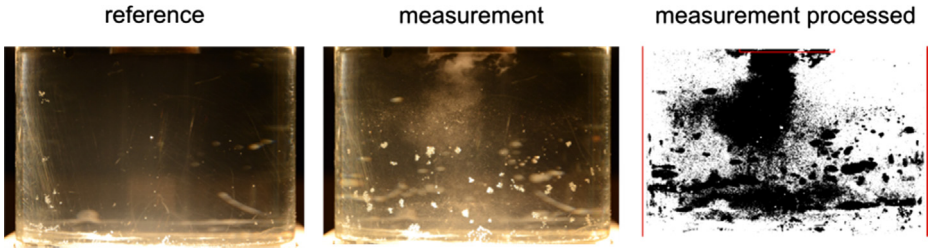

Fig. 5. Image processing procedure: left: reference; middle: photo during measurement; right: resulting black and white picture (red lines indicate the container walls and horn position). (For interpretation of the references to color in this figure legend, the reader is referred to the web version of this article.)

degree of brightness. Before ultrasound was switched on, a reference photo was recorded for every measurement series. This was done in order to determine the differences caused by the sonication. The image processing procedure is shown in Fig. 5. By subtracting the reference photo from the pictures taken during the measurements, the changes caused by ultrasound irradiation and cavitation can be visualized. The resulting black and white image shows the cavitation activity inside the container. The black pixels correspond to cavitation bubbles. The horn's position and the container walls are indicated by red lines.

The reference photo shows few small air bubbles inside the fluid and trapped on the container wall. Scratches on the container are also visible. The measurement photo not only shows cavitation bubbles inside the liquid, but additional bubble clusters on the container wall as well. These are indicated by big bright spots in the foreground and background. In the processed photo, the bubbles on the container wall are also converted to black pixels and are therefore counted as bubble content.

In order to get an impression of the amount of cavitation activity and the spatial cavitation distribution, the acquired photo data were compiled into an overview picture for every measurement series. These overview pictures show where cavitation occurs and the intensity of the occurrence. By compiling the individual black-and-white images, a gray scale image is generated. Here the cavitation occurrence rate (how often the pixels were black) is displayed. These images show the local cavitation occurrence distribution. This allows an evaluation of the spectrograms and the affiliated gray scale pictures, in order to correlate the cavitation field structure and intensity with the frequency portions in the spectrograms. The following figures show the significant changes in cavitation activity and the measured frequency fractions for the four different immersion depths. In Fig. 6 the most striking changes during the evolution of cavitation activity can be seen for a distance of 80 mm between container bottom and the horn's tip. By increasing the excitation amplitude up to 1000 mA, no major changes occur in the fluid. A few isolated small bubble clouds are present, and bigger bubbles

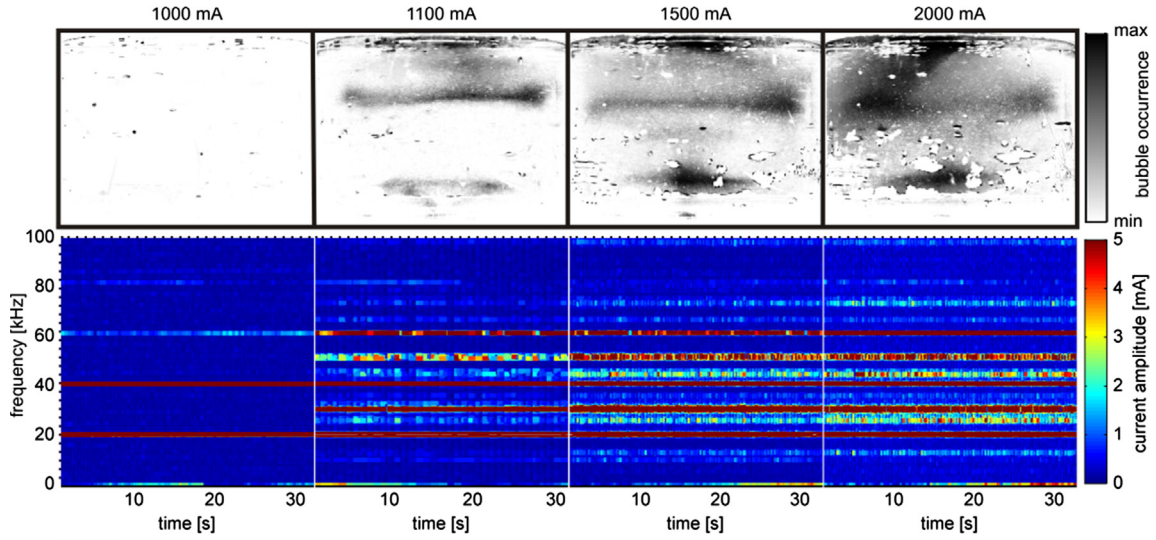

Fig. 6. Cavitation activity indicated by gray scale images and spectrograms for a distance of 80 mm.

trapped on the container wall vibrate continuously around their position leading to black spots. In addition, some bubbles travel around the fluid by streaming effects and cause gray stripes in the gray scale picture. The corresponding spectrograms show elevated amplitudes mainly for the driving frequency, its harmonics and a low frequency portion. A further increase in excitation amplitude, to 1100 mA, suddenly leads to the occurrence of cavitation bubbles in the upper and lower half of the container in two separate zones, while more bubbles occur in the upper half. The corresponding spectrogram shows a highly elevated distinct frequency fraction at $3/2f_0$ (~30 kHz) and an elevated band at $5/2f_0$ (~50 kHz), which is wider than the $3/2f_0$ (~30 kHz) portion.

The third harmonic ($3f_0$, ~60 kHz) shows higher values than in the measurements before, and additional subharmonics and ultraharmonics appear with slightly increased intensities, varying over the measurement time. Grayscale picture and spectrogram show that a cavitation threshold has been exceeded.

By a further increase in excitation amplitude, the two zones of bubble occurrence enlarge until at 2000 mA, when cavitation bubbles are generated almost everywhere in the liquid. For all measurements, the strongest cavitation occurrences can be observed at the horn's tip, at the lower end of the upper occurrence zone and at the center of the lower zone near the container bottom. The big white spots in the gray scale pictures of 1500 mA and 2000 mA originate from bubbles, which were already stuck to the container wall when the reference photo was taken and didn't disappear during the measurement. The measurements for the different excitation amplitudes were carried out successively, so bubbles generated during a measurement are present on the reference photo of the following measurement. This leads to white spots after the image processing. The dark borders surrounding the bright spots correspond to smaller bubbles, which are attached to the main bright bubble, vibrating on the container wall.

In the spectrograms for the increased excitation amplitudes, the frequency band around the $3/2f_0$ (~30 kHz) fraction widens and an additional frequency range at $5/4f_0$ (~25 kHz) shows elevated amplitudes over the whole measurement time. The $5/2f_0$ (~50 kHz) band shows higher amplitudes than before and additional elevated amplitudes can be found for a band at $9/4f_0$ (~46 kHz).

For the highest excitation amplitude of 2000 mA, the $5/4f_0$ (~25 kHz) band widens and connects to the $3/2f_0$ (~30 kHz) fraction and a $7/2f_0$ (~72 kHz) portion becomes more pronounced.

The first change in the horn's immersion depth doesn't significantly change the cavitation occurrence, but affects the amplitude levels that lead to changes in cavitation generation. Fig. 7 shows grayscale images and spectrograms for a distance of 75 mm between container bottom and horn's tip.

For excitation amplitudes up to 1400 mA, no major changes occur in the fluid. Only few small bubble clouds appear temporarily, mainly in the lower half of the container. Also, movement of the water surface is made visible by a dark rim at the top of the image for 1400 mA. An excitation amplitude of 1500 mA leads to the formation of two separate zones, in which cavitation bubbles occur. A further increase in excitation amplitude enlarges these zones. Again, the upper zone is bigger than the lower one. The spectrograms generally show the same frequency portions as for 80 mm distance. When the cavitation threshold is exceeded at 1500 mA, the $9/4f_0$ (~46 kHz) frequency portion is more pronounced than for 80 mm. The fourth harmonic ($4f_0$) appears with high amplitudes for 2000 mA.

Decreasing the distance between horn's tip and container bottom to 70 mm has more influence on the cavitation occurrence than the previous distance change. Fig. 8 shows the corresponding gray scale images and spectrograms. Already for 500 mA there is a small conical zone where cavitation occurs present around the horn's tip, while there is little cavitation directly at the tip. Although cavitation is generated, the indicators observed so far are not present in the frequency spectrum. For amplitude levels of 1300 mA and higher, the $3/2f_0$ (~30 kHz), $5/2f_0$ (~50 kHz) and $9/4f_0$ (~46 kHz) frequency portion appear for different time spans, but not for the whole measurement time. The next significant change appears for 1700 mA. Cavitation bubbles temporarily appear to be widely distributed in the container. The highest bubble occurrence is found at the top of the liquid, but compared to the previous immersion depths, few cavitation bubbles appear. Still, there is very little cavitation activity directly at the horn's tip. The only frequency portion that is present during the whole measurement and deviates from the harmonics is the $9/4f_0$ (~46 kHz) component. The $3/2f_0$ (~30 kHz) and $5/2f_0$ (~50 kHz) component appear a few times for a very short period. Higher excitation amplitudes, again, lead to the formation of two separated zones, where lots of cavitation bubbles appear with the highest occurrence at the horn's tip.

This is accompanied by the presence of the $5/4f_0$ (~25 kHz), $3/2f_0$ (~30 kHz), $5/2f_0$ (~50 kHz), $13/4f_0$ (~67 kHz) and the $17/4f_0$ (~87 kHz) portions as well as the fourth harmonic with high amplitudes over the whole measurement time. The $f_0/2$ (~10 kHz) and $7/2f_0$ (~72 kHz) portions also become more pronounced for high currents. It is noticeable that for 2000 mA the $13/4f_0$ (~67 kHz) and the $17/4f_0$ (~87 kHz) portion are shifted to higher frequencies, while the frequency of the fourth harmonic is slightly lower than before. This may be due to the nonlinearity of the ultrasonic system, which is amplitude dependent. Subharmonic content at approximately $0.65f_0$ is also

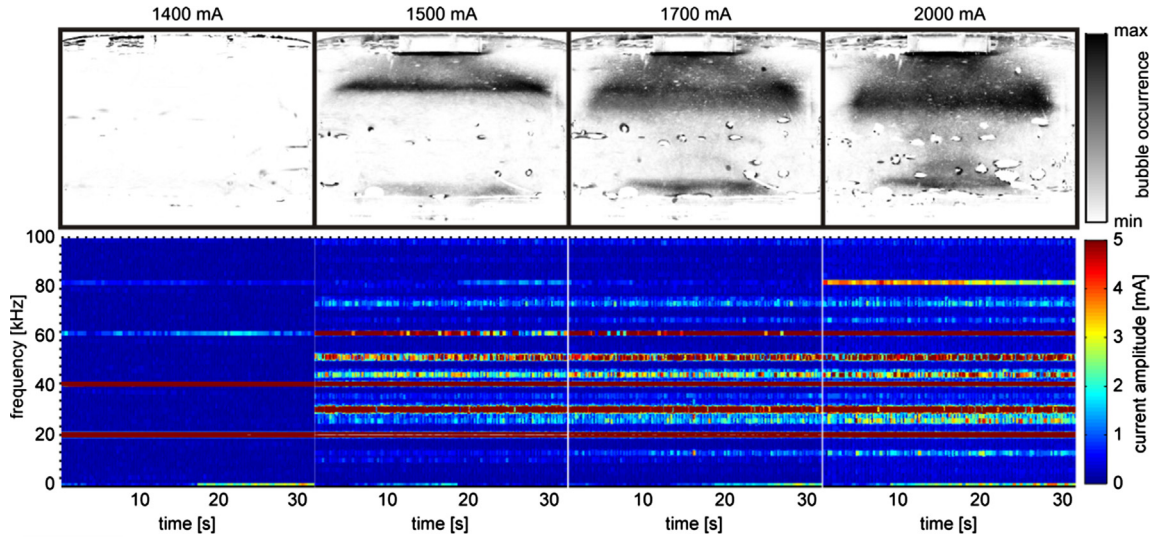

Fig. 7. Cavitation activity indicated by gray scale images and spectrograms for a distance of 75 mm.

generated.

For a distance of 65 mm, more changes in cavitation occurrence, and the affiliated frequency spectra can be observed than for the three distances already discussed (see Figs. 9 and 10).

For all measurements up to 900 mA, the spectrograms show elevated amplitudes for $9/2f_0$ (~93 kHz). This frequency portion is not cavitation related. It is even present at times when the ultrasound is switched off (not shown here).

The origin of this phenomenon is not yet confirmed. It is assured that the $9/2f_0$ (~93 kHz) portion that is found in spectrograms for excitation amplitudes higher than 900 mA is cavitation related. While at 100 mA, bubbles already start traveling through the fluid and occasionally appear in a cluster beneath the horn's tip. For 300 mA cavitation, bubbles appear in a conical zone, like for 500 mA at 70 mm distance. In addition to harmonics now the $7/2f_0$ (~72 kHz) portion appears in the spectrogram.

While the cavitation structure does not change when the excitation amplitude is increased, the number of elevated frequency portions increases until 900 mA is reached. For this excitation, the cavitation bubbles are more widely distributed with a small zone of high occurrence at the center of the horn's tip. Some of the frequency portions, which were present before, also disappear and, besides harmonics, the frequency component showing the highest amplitudes is the $7/2f_0$ (~72 kHz). The next major change appears for 1300 mA. Here the cavitation structure changes again and the frequency indicators suggest that a cavitation threshold has been exceeded. The highest bubble occurrence is on the left side of the horn and bubbles appear more frequently in the lower half of the container. The spectrogram shows frequency content similar to the spectrograms for high excitation amplitudes for the other immersion depths with an additional $19/4f_0$ (~98 kHz) component. Increasing the excitation first leads to the formation of a large zone with high bubble occurrence at the tip of the horn, which evolves into a beam like structure towards the container bottom. The $19/4f_0$ (~98 kHz) component disappears and the spectrograms show the same frequencies as for high amplitudes at 70 mm distance.

The results presented here show that the generation of ultraharmonics with amplitude values equal to or higher than 5 mA can be linked to the generation of transient cavitation. The cavitation bubble distribution is highly dependent on geometric boundary conditions, which are influenced most by immersion depth.

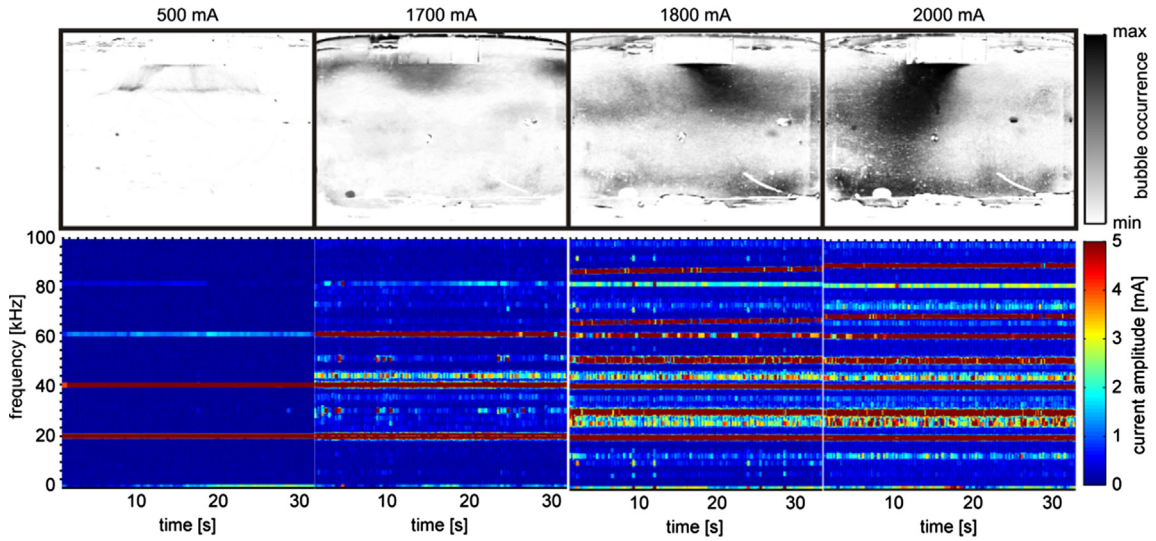

Fig. 8. Cavitation activity indicated by gray scale images and spectrograms for a distance of 70 mm.

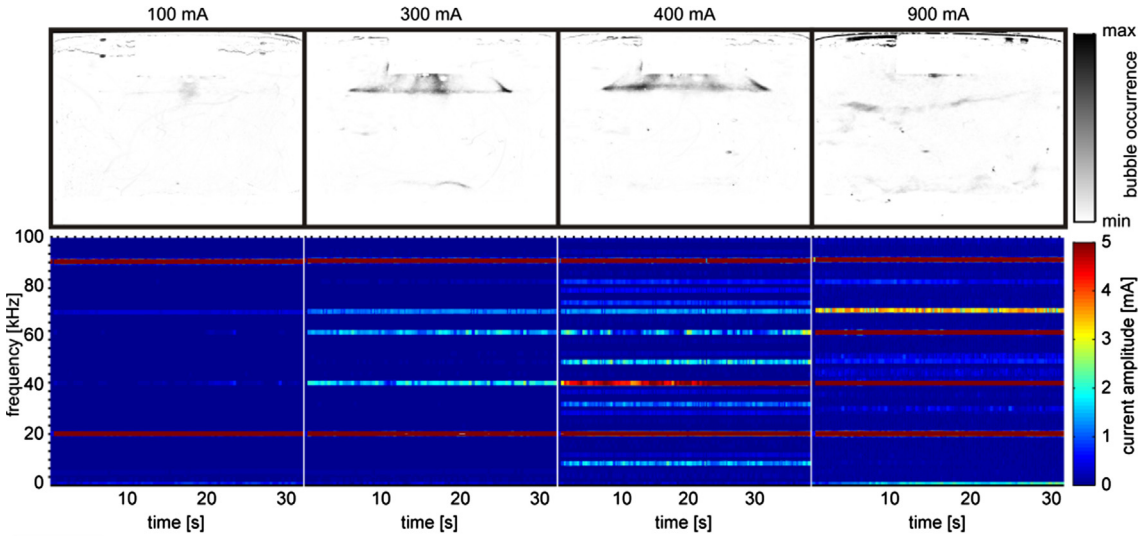

Fig. 9. Cavitation activity indicated by gray scale images and spectrograms for a distance of 65 mm.

5. Correlation between cavitation intensity and frequency based indicators

It has already been shown that, by the operation of the transducer itself without a load, and depending on the excitation amplitude, different frequency components are present in the current signal. Therefore, it is necessary to investigate which relationships between cavitation intensity and frequency-based indicators can be found despite the sensor characteristics. The cavitation intensity is determined by the number of pixels corresponding to cavitation activity. The number of cavitation bubbles, determined from the photographs, has to be considered erroneous for various reasons: (1) the photos only show part of the container; (2) image processing identifies changes in relation to a reference picture, which leads to relative instead of absolute values; (3) bubbles sticking to the container wall prevent insight into parts of the container; (4) the bubbles have different size, so the number of pixels is not equal to the number of cavitation bubbles.

Nevertheless, the determined cavitation activity can be considered representative, as differences between the measurements are shown.

In order to determine if there is a correlation between the determined pixel number and frequency components, the mean pixel number is calculated for all current intensities for all four distances. The results are shown in Fig. 11(a). The $3/2f_0$ (~30 kHz) frequency component and two low-frequency bands were chosen as potential cavitation indicators. The evaluation of the photo study showed good agreement between the generation of cavitation bubbles and the appearance of this frequency component. The two low frequency bands are investigated because broad band noise is known to be an indicator for transient cavitation. The ranges of the low-frequency bands are 0.5–12.5 kHz and 14–19 kHz. These bands represent broadband noise below the excitation frequency. The gap between both bands ensures that the $0.65f_0$ (~13 kHz) frequency component, which occurs with

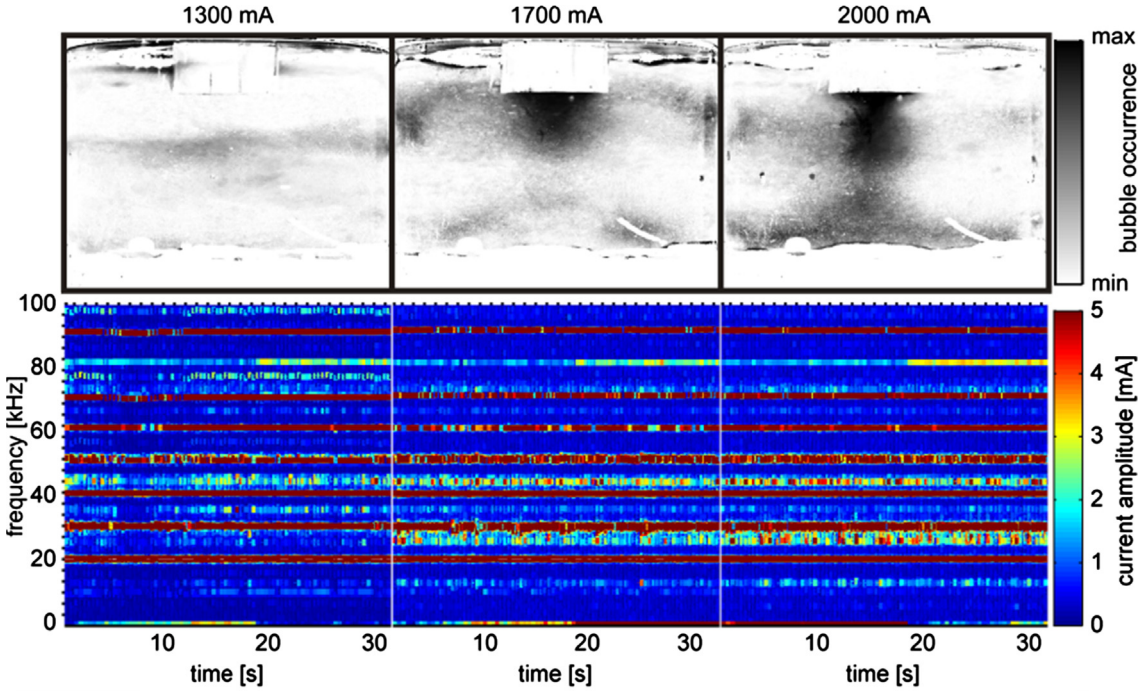

Fig. 10. Cavitation activity indicated by gray scale images and spectrograms for a distance of 65 mm.

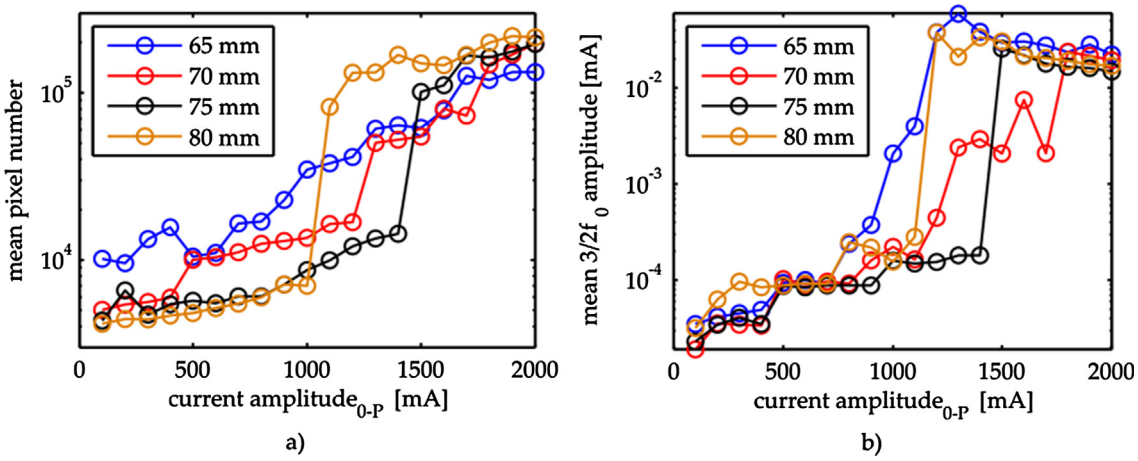

Fig. 11. Mean values for all current amplitudes and distances: (a) mean pixel number; (b) mean $3/2f_0$ amplitude.

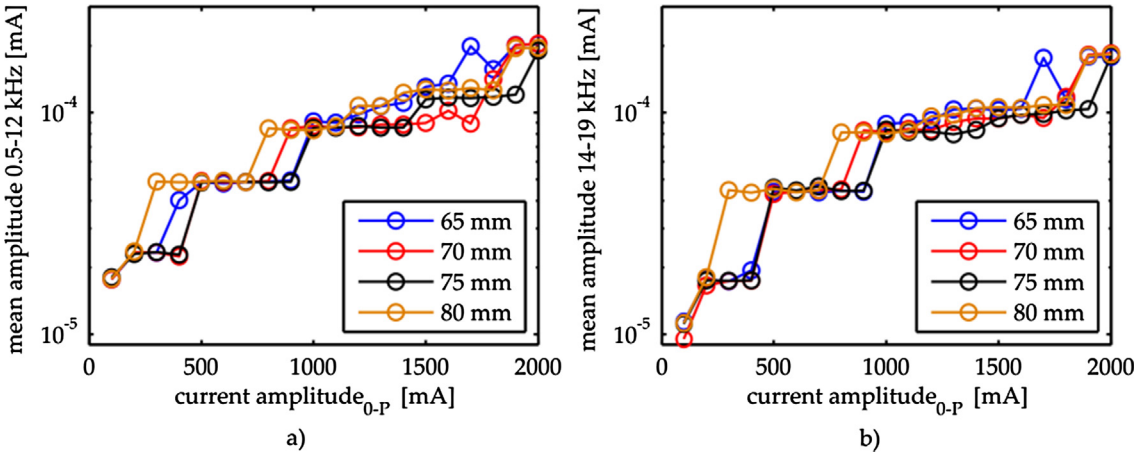

Fig. 12. Mean amplitudes for two frequency bands below the driving frequency: (a) 0.5–12.5 kHz; (b) 14–19 kHz.

some measurements, is not considered. The evaluation of the $3/2f_0$ (~30 kHz) fraction is shown in Fig. 11(b). Fig. 12 shows the evaluation of the two low frequency bands.

The most distinct increase in pixel number occurs at a distance of 80 mm, as the excitation current amplitude exceeds 1000 mA, and at a distance of 75 mm, as soon as 1400 mA is exceeded. The $3/2f_0$ (~30 kHz) component shows the same behavior as the pixel number for 75 mm. For 80 mm, the strong increase occurs when 1100 mA are exceeded. It is assumed that this distinct increase indicates that the transient cavitation threshold has been exceeded. The link between the thresholds, detected with the self-sensing approach, and the onset of transient cavitation was established by visual observations of cavitation events and structures known to occur in transient cavitation. In addition, changes in audible noise also indicated the onset of transient cavitation.

The mean pixel number shows bigger increases for 500 mA, 1300 mA and 1800 mA. This behavior is also found for the corresponding curve of the $3/2f_0$ (~30 kHz) indicator. From the photo study, the appearance of jellyfish cavitation structures [19] can be associated with the increase for 1300 mA. This indicates that the transient cavitation threshold has been exceeded. The most gradual increase in pixel number occurs at a distance of 65 mm. More pixels are present here, for low current amplitudes, than for the other distances, while the maximum pixel number, at high amplitudes, is the lowest. Although cavitation structures are already generated beginning at 300 mA for amplitudes below 1000 mA, there seems to be no correlation between pixel number and the cavitation indicator. At 1000 mA, the transient cavitation threshold seems to be exceeded, as the value of the frequency component increases drastically.

The $3/2f_0$ (~30 kHz) frequency component shows a decreasing tendency for all distances after exceeding the transient cavitation threshold. It is assumed that, from that point on, energy is transferred to further frequency components.

In Fig. 12, the mean amplitude values for two frequency bands below the driving frequency are shown for all measurements. These bands represent a broad band noise level. Fig. 12(a) shows the frequency band 0.5–12.5 kHz and the 14–19 kHz band is shown in Fig. 12(b). For low excitation amplitudes, both graphs show no strong correlation with the mean pixel number. It is assumed that the noise levels in this region are highly influenced by the frequency content generated by driving the transducer. Once the individual transient cavitation thresholds have been exceeded, the graphs show more individual changes and a good correlation with the mean pixel number. In order to better illustrate this relationship, Figs. 13 and 14 show the two bands in comparison with the cavitation activity in the range above 1000 mA for the individual distances. Although the values for both frequency bands tend to change more drastically for high amplitudes than the cavitation activity, a general similarity is recognizable. It is assumed that the increase in noise level here is mostly influenced by transient cavitation induced broad band noise.

6. Conclusion and discussion

For detection of ultrasonic generated cavitation, a novel self-sensing method was used, that can be applied even under hard to access or opaque conditions. It has been shown that using this method, cavitation

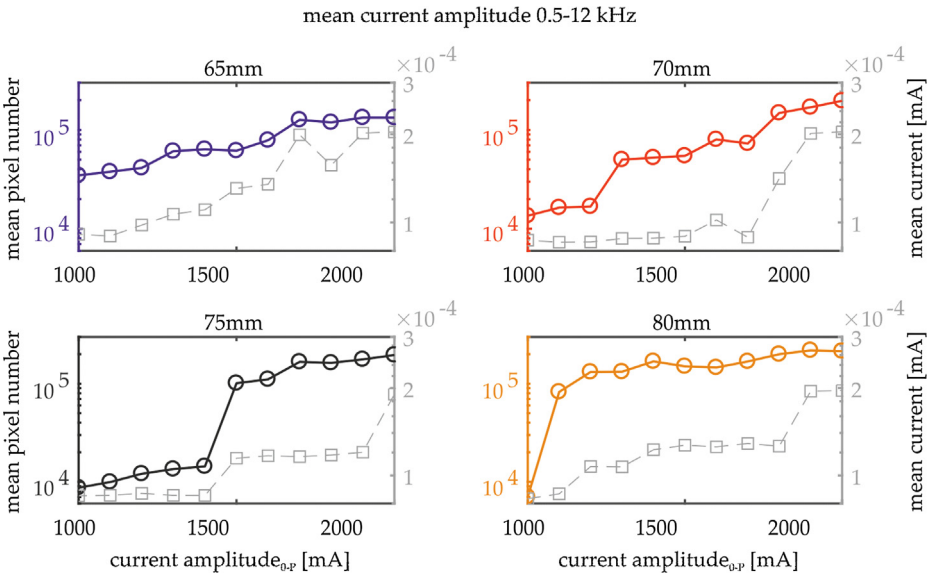

Fig. 13. Detailed comparison of the mean pixel number (cavitation activity) and the mean current amplitude in the frequency band 0.5–12 kHz.

can be detected without any further measurement devices. In additional measurements, that are not presented here, this technique has been applied to an ultrasound assisted casting process with aluminum melt. In these experiments the occurrence of different frequency components in the current signal could also be linked to the generation of cavitation.

In order to obtain a conclusion on the cavitation processes in the liquid, a photo study was additionally performed.

The investigation of the characteristic frequency components, generated by driving the transducer, showed that several frequency portions known as acoustic cavitation indicators, such as harmonics of the driving frequency, a low frequency portion and the global noise level, are part of the system's characteristic and therefore make cavitation detection more difficult.

The occurrence of ultraharmonics in the frequency spectrum was identified as an indicator of cavitation activity, for all investigated test arrangements. The excitation amplitude, for which the threshold for cavitation generation was reached, varied with the distance between container bottom and horn's tip.

The number of the occurring ultraharmonics also varied with the immersion depth of the horn. For smaller distances, a higher submerging level, therefore more ultraharmonics appeared in the spectrum. This can be explained with the larger horn surface area that is influenced by cavitation activity for higher submerging levels. If a larger area is influenced by cavitation, the intensity of the frequency portions present is increased. In addition, the increasing number of ultraharmonics can be related to the different structures of the resulting cavitation fields. For higher submerging levels, the horn is influenced not only on the tip face, but also on the sides by cavitation.

The fact that different results were achieved for different experimental conditions supports the conclusion of preceding studies, that changes in the experimental set-up change the self-sensing results.

Elevated values of the $3/2f_0$ (~30 kHz) frequency portion were identified as an indicator for the onset of transient cavitation. This indicator was also found by other researchers. Once the transient cavitation threshold has been exceeded, the cavitation intensity shows good correlation with broad band noise levels in two frequency bands below the driving frequency. This link has not been reported by other researchers and underlines the dependence of the self-sensing technique

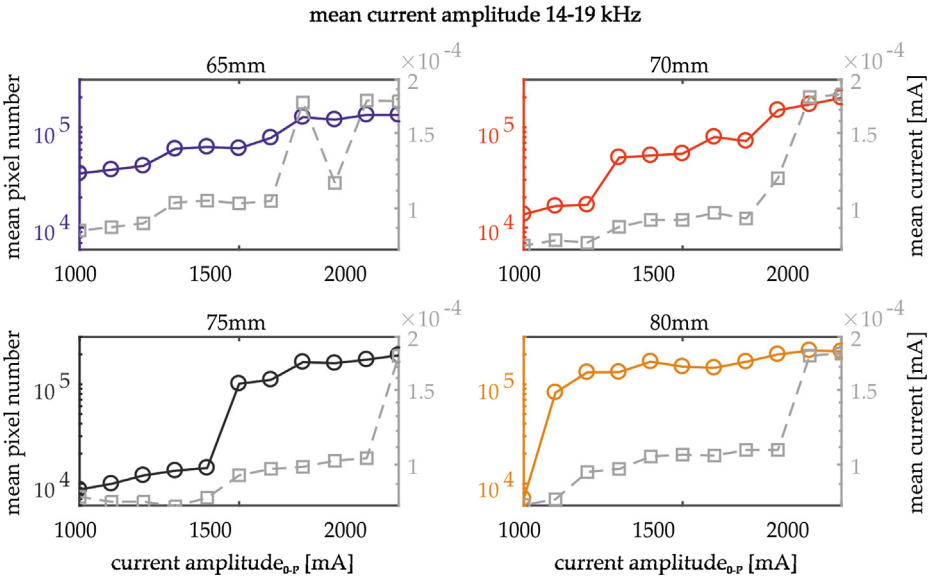

Fig. 14. Detailed comparison of the mean pixel number (cavitation activity) and the mean current amplitude in the frequency band 14–19 kHz.

on the experimental setup and the transducers frequency characteristic.

The results presented in this study are valid for the presented experimental setup. It is probable that the detectable frequency components, and the sensitivity towards them, are dependent on the characteristics of the ultrasound system and thus on the geometry of the transducer. Therefore, it is necessary to investigate the differences that occur when another ultrasonic transducer or when other electrical components are used. A change in experimental setup may also influence the sensitivity of the self-sensing process.

It should also be investigated how a change in the sonoreactor's geometry affects the results.

With the presented results, an advance towards cavitation detection in rough process environments has been made. However, further studies are necessary in order to make it possible to control the cavitation process by means of the identified indicators.

Funding

This work was supported by DFG (Deutsche Forschungsgemeinschaft) [grant numbers BA 851/114-1/WA 564/28-1].

References

[1] K.A. Saalbach, P. Freytag, K. Kerber, J. Twiefel, Ultrasonic assisted simultaneous composite casting-A feasibility study, Ultrasonics Symposium (IUS), 2012 IEEE International, IEEE, 2012, pp. 775–777, , http://dx.doi.org/10.1109/ULTSYM.2012.0193.

[2] K.A. Saalbach, P. Freytag, K. Kerber, J. Twiefel, Bond quality investigation of ultrasonic assisted composite casting, in: IWPMA & EHW, 14.-18.07.2013: 10th International Workshop of Piezoelectric Materials and Applications in Actuators, 8th Annual Energy Harvesting Workshop, Hannover, 2013, doi: 10.2314/IWPMA_45.

[3] P. Bornmann, et al., Non-perturbing cavitation detection/monitoring in sonochemical reactors, Ultrasonics Symposium (IUS), 2012 IEEE International, IEEE, 2012.

[4] P. Bornmann, et al., Self-sensing ultrasound transducer for cavitation detection, Ultrasonics Symposium (IUS), 2014 IEEE International, IEEE, 2014.

[5] Saalbach Kai-Alexander, Twiefel Jens, Wallaschek Jörg, Self–sensing cavitation detection capability of horn geometries for high temperature application, J. Vibroeng. 18 (2) (2016) 989–998.

[6] P. Bornmann, T. Hemsel, W. Sextro, G. Memoli, M. Hodnett, B. Zeqiri, Kavitationsdetektion mittels Self-Sensing-Ultraschallwandler, Tm - Technisches Messen 82 (2) (2015) 73–84, http://dx.doi.org/10.1515/teme-2015-0017.

[7] E. Cramer, W. Lauterborn, Acoustic cavitation noise spectra, Appl. Sci. Res. 38 (1982) 209–214.

[8] M. Ashokkumar, M. Hodnett, B. Zeqiri, et al., Acoustic emission spectra from 515 kHz cavitation in aquenous solutions containing surface-active solutes, J. Am. Chem. Soc. 129 (2007) 2250–2258.

[9] P.W. Vaughan, Investigation of acoustic cavitation thresholds by observation of the first subharmonic, J. Sound Vibrat. 7 (2) (1968) 236–246.

[10] M.R. Bailey, et al., Cavitation detection during shock-wave lithotripsy, Ultrasound Med. Biol. 31 (9) (2005) 1245–1256, http://dx.doi.org/10.1016/j.ultrasmedbio.2005.02.017 ISSN 0301-5629.

[11] J. Frohly, et al., Ultrasonic cavitation monitoring by acoustic noise power measurement, J. Acoust. Soc. Am. 108 (5) (2000) 2012–2020.

[12] P. De Santis, D. Sette, F. Wanderlingh, Cavitation detection: the use of the subharmonics, J. Acoust. Soc. Am. 42 (2) (1967) 514–516.

[13] M. Čdina, Detection of cavitation phenomenon in a centrifugal pump using audible sound, Mech. Syst. Signal Process. 17 (6) (2003) 1335–1347, http://dx.doi.org/10.1006/mssp.2002.1514 ISSN 0888-3270.

[14] D. Samah, P.T. Sinaptec, J.-F. Rouchon, Influence of cavitation on ultrasonic piezoelectric transducers impedance: Modelling and experimentation, in: Electronics, Control, Measurement, Signals and Their Application to Mechatronics (ECMSM), 2013 IEEE 11th International Workshop of, (2), 2013, Retrieved from <http://ieeexplore.ieee.org/xpls/abs_all.jsp?arnumber=6648960>.

[15] K.S. Van Dyke, The piezo-electric resonator and its equivalent network, Proc. Inst. Radio Eng. 16 (6) (1928) 742–764, http://dx.doi.org/10.1109/JRPROC.1928.221466.

[16] I. Ille, J. Twiefel, Model-based feedback control of an ultrasonic transducer for ultrasonic assisted turning using a novel digital controller, Phys. Procedia 70 (2015) 63–67.

[17] J. Twiefel, et al., Digital signal processing for an adaptive phase-locked loop controller, The 15th International Symposium on: Smart Structures and Materials & Nondestructive Evaluation and Health Monitoring, International Society for Optics and Photonics, 2008.

[18] W. Littmann, T. Hemsel, C. Kauczor, J. Wallaschek, M. Sinha, Load-adaptive phase-controller for resonant driven piezoelectric devices (2003) 547–550.

[19] R. Mettin, et al., Bubble structures in acoustic cavitation: observation and modelling of a'jellyfish'-streamer, in: Forum Acusticum Sevilla, 2002.